Comparison of Gold Nanoparticle Mediated Photoporation: Vapor Nanobubbles Outperform Direct Heating for Delivering Macromolecules in Live Cells

Ranhua Xiong,[†,‡] Koen Raemdonck,[†] Karen Peynshaert,[†] Ine Lentacker,[†] Ine De Cock,[†] Jo Demeester,[†] Stefaan C. De Smedt,[†] Andre G. Skirtach,[‡,§,∥] and Kevin Braeckmans[†,‡,*]

[†]Laboratory of General Biochemistry and Physical Pharmacy, Ghent University, Harelbekestraat 72, 9000 Ghent, Belgium, [‡]Centre for Nano- and Biophotonics, Ghent University, Harelbekestraat 72, 9000 Ghent, Belgium, [§]Department of Molecular Biotechnology, Ghent University, 9000 Ghent, Belgium, and [∥]Max-Planck Institute of Colloids and Interfaces, 14424 Potsdam, Germany

ABSTRACT There is a great interest in delivering macromolecular agents into living cells for therapeutic purposes, such as siRNA for gene silencing. Although substantial effort has gone into designing nonviral nanocarriers for delivering macromolecules into cells, translocation of the therapeutic molecules from the endosomes after endocytosis into the cytoplasm remains a major bottleneck. Laser-induced photoporation, especially in combination with gold nanoparticles, is an alternative physical method that is receiving increasing attention for delivering macromolecules in cells. By allowing gold nanoparticles to bind to the cell membrane, nanosized membrane pores can be created upon pulsed laser illumination. Depending on the laser energy, pores are created through either direct heating of the AuNPs or by vapor nanobubbles (VNBs) that can emerge around the AuNPs. Macromolecules in the surrounding cell medium can then diffuse through the pores directly into the cytoplasm. Here we present a systematic evaluation of both photoporation mechanisms in terms of cytotoxicity, cell loading, and siRNA transfection efficiency. We find that the delivery of macromolecules under conditions of VNBs is much more efficient than direct photothermal disturbance of the plasma membrane without any noticeable cytotoxic effect. Interestingly, by tuning the laser energy, the pore size could be changed, allowing control of the amount and size of molecules that are delivered in the cytoplasm. As only a single nanosecond laser pulse is required, we conclude that VNBs are an interesting photoporation mechanism that may prove very useful for efficient high-throughput macromolecular delivery in live cells.

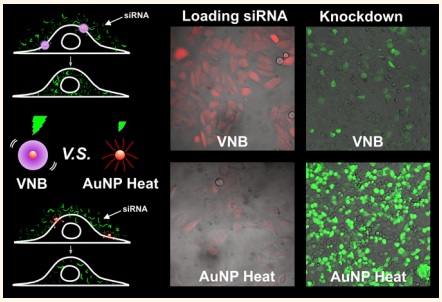

KEYWORDS: gold nanoparticles · vapor nanobubbles · photoporation · intracellular delivery · siRNA · knockdown efficiency

For many therapeutic applications, macromolecules need to be delivered into living cells.[1] For example, to allow sequence-specific gene silencing on the post-transcriptional level, small interfering RNA (siRNA) needs to be delivered into the target cell's cytoplasm.[2] This is typically achieved by means of formulating the siRNA into nonviral lipid or polymer nanocarriers. As these are generally internalized by cells through endocytosis, escape from the endosome and subsequent siRNA release is needed. However, to date, endosomal escape remains one of the major bottlenecks hampering safe and efficient delivery of therapeutic macromolecules into the cytosol.[3,4]

As an alternative strategy, physical approaches to permeate the cell membrane have attracted considerable interest, especially for *in vitro* applications. They typically offer generic applicability to a variety of cell types and grant macromolecular agents such as siRNA direct access into the cytoplasm.[5−7] A first example is microinjection, a conventional tool to directly inject compounds into single cells.[8−10] However, this technique can be applied only to a limited number of cells and typically requires a skilled person to perform. Electroporation is another common physical technique to deliver molecules into cells *in vitro* and *in vivo*. While it has shown to lead to good transfection efficiencies,[11−15]

* Address correspondence to Kevin.Braeckmans@UGent.be.

Received for review April 1, 2014 and accepted May 28, 2014.

Published online May 28, 2014
10.1021/nn5017742

the high electric field often results in low cell viability.[16,17] More recently, sonoporation has been introduced as a method to permeabilize the plasma cell membrane by making use of ultrasound-responsive microbubbles. The acoustic response of the microbubbles can lead to the formation of microjets and shockwaves, resulting in cell membrane poration.[18,19] However, shear forces or elevated temperatures can lead to substantial cell damage and toxicity.[20,21]

Photoporation is an alternative physical approach that has received increasing attention in recent years. In its most straightforward form, cell membrane permeability is obtained by focusing high-intensity femtosecond laser pulses onto individual cells.[22−28] By attaching plasmonic nanoparticles, such as gold nanoparticles (AuNPs), to the cell membrane, the photoporation effect can be achieved at lower laser intensities. This means that throughput can be increased since nonfocused laser light can be used to illuminate a large amount of cells.[29−31] This is thanks to the AuNP surface plasmon resonance (SPR), which depends on the size, shape, and surface coating of the particles, which tremendously enhances laser absorption,[30,32,33] leading to distinct phenomena such as heating of the surrounding tissue, acoustic shockwaves, and formation of water vapor nanobubbles (VNBs).[30,34] Recently, it has been shown that both heating and VNBs can be used to permeate the plasma membrane and deliver cell-impermeable compounds into the cytosol.[35−37] For heating of the plasma membrane, both continuous wave (CW) and low-intensity pulsed laser light have been employed to heat membrane-adsorbed AuNPs, resulting in pore formation by a local phase transition of the lipid bilayer or by thermal denaturation of integral glycoproteins.[35−38] However, diffusion of heat throughout the cell can result in hyperthermia-induced cell stress, substantially decreasing cell viability.[35,37] When using short laser pulses (<10 ns) of sufficiently high intensity, the temperature of a AuNP can rapidly increase to several hundred degrees, due to which the water surrounding the AuNP evaporates, resulting in a VNB that emerges around its surface.[30,39] The size of a VNB can be tuned from ten to several hundreds of nanometers depending on the laser intensity.[32,40] When the thermal energy of the AuNP is consumed, the VNB violently collapses and causes local damage by high-pressure shockwaves. Due to the extremely short lifetime of VNBs (<1 μs), the diffusion of heat from the AuNP into the environment is negligible, so that almost all energy of the irradiated AuNP is converted to mechanical energy (expansion of the VNB) without heating of the environment. This property makes VNBs an interesting phenomenon to cause local mechanical damage, without causing thermal damage to the surrounding healthy tissue. It has been shown that VNBs can induce membrane pores through which compounds can diffuse into the cell.[41,42] Thus, direct heating and VNB formation by laser-irradiated AuNPs are two distinct photothermal effects that can be used to deliver cell-impermeable compounds directly into the cytosol. However, to date it remains unclear which of the two effects is preferred in terms of delivery efficiency and cytotoxicity. Neither has it been evaluated if VNB-induced membrane poration can be used to deliver siRNA into cells.

Here we report on a systematic comparison of AuNP-mediated photoporation for delivering macromolecules in cells by direct heating and VNB generation. Despite the fact that it requires higher laser energies, surprisingly we find that VNBs allow more efficient cellular uptake of compounds with little or no cytotoxicity as compared to direct heating. Furthermore, we successfully show that VNB photoporation can more efficiently transfect cells with siRNA compared to direct heating, resulting in enhanced target gene silencing. Finally, we show that pores of different sizes can be created depending on the laser energy, thus enabling size-selective delivery of macromolecules in cells. On the basis of these results we envisage that VNB photoporation can offer unique opportunities for drug delivery in live cells.

RESULTS AND DISCUSSION

Cell-Adsorbed AuNPs Mediate Distinct Photothermal Effects as a Function of Laser Fluence. The experimental procedure to load cells with cell-impermeable molecules is shown in Figure 1. First, AuNPs are adsorbed onto the cell's surface, by which they can act as mediators of nanopore formation. In this study, positively charged AuNPs (70 nm) were used to facilitate interaction with the negatively charged cell membrane. Following incubation of HeLa cells with three different AuNP concentrations (4.1×10^7, 8.2×10^7, and 16.5×10^7 particles/mL) for half an hour at 37 °C, the number of cell-attached AuNPs was quantified from confocal images in reflection mode. As shown in Figure S1a−c, more AuNPs adsorbed to the cells with increasing concentrations of AuNPs, ranging from 4 to approximately 15 particles per cell. In the second step of the procedure, the nonadherent AuNPs are removed and the cell-impermeable molecules are added to the cells just prior to the laser treatment. A low laser energy will lead to heating of the cell membrane, while VNBs are formed at higher laser energies. The two effects can be monitored by detecting the transmitted intensity of a CW laser focused on the sample (Figure S2).[32] Heating of a AuNP induces a local change in refractive index.[43] This "thermolensing" effect can cause a refocusing of the CW laser on the pinhole in front of the detector (as shown in Figure S2), resulting in an increase of the detected transmitted CW laser light. A laser pulse with energy below the VNB threshold will cause heating of

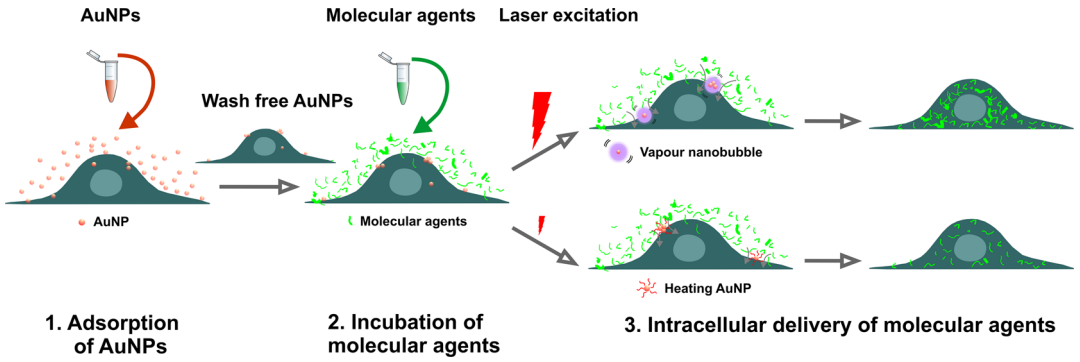

Figure 1. Schematic overview of the experimental procedure. 1. Cells are incubated with AuNPs that are adsorbed to the cell membrane. 2. The nonadherent AuNPs are removed in a washing step, after which the solution of molecular agents is added to the cells just prior to the laser treatment. 3. Laser treatment causes pore formation either by VNBs that mechanically puncture the cell membrane (high laser energy) or by heating of the cell membrane (low laser energy). The extracellular molecules are finally expected to diffuse into the cells *via* the created pores.

the AuNP, after which this heat diffuses into the environment. The corresponding intensity profile of the transmitted laser light is shown in Figure S3a. The long tail is indicative of heat diffusion and heating of the environment. At a pulse energy above the VNB threshold, VNBs are created with a size and lifetime that is proportional to the laser energy (Figure S3b and c). The absence of a heat diffusion tail at high pulse energies clearly demonstrates that VNB generation does not cause heat transfer to the environment. Alternatively, VNBs can be detected by dark-field microscopy, as demonstrated in Figure S2d–f.[44] From these experiments we can conclude that VNBs could be clearly generated at a laser fluence of 1.02 J/cm^2, while 0.38 J/cm^2 resulted only in heating of the surrounding medium. This result is in agreement with the threshold of VNB generation as reported before under similar conditions.[32] It is of note that the medium surrounding the AuNPs can affect the threshold for the generation of gas bubbles.[45]

Intracellular Delivery of Macromolecules and Cell Viability *via* Local Heating or VNB Generation. FITC-dextran with a molecular weight of 10 kDa (FD10) was used as a model macromolecule to compare cell loading by direct heating or VNB generation. We use the term "cell loading" to signify delivery of macromolecules into cells across the plasma membrane by VNB-induced membrane pores. For an AuNP concentration of 8.2 × 10^7 particles/mL (*i.e.*, approximately 8 AuNPs per cell; Figure S1d), two different laser fluence levels were tested, *i.e.*, one below (0.38 J/cm^2) and one above the VNB threshold (2.04 J/cm^2). All cells in a well of a 96-well titer plate were treated with a single laser pulse of the indicated energy. After laser treatment the cells were washed immediately to remove the remaining extracellular FITC-dextran, and fresh cell medium was added to avoid the endocytosis of FITC-dextran. Just as for other poration techniques (microinjection, electroporation, sonoporation, direct photoporation) the pores generated by the bubbles are also quickly repaired in a few tens of seconds, as shown in very recently studied vapor bubble mediated poration.[46] Calcein red-orange AM was added to the cells to quantify cell viability. The images presented in Figure 2 clearly show that FITC-dextran loading was much more efficient when mediated by VNBs than by direct heating of the plasma membrane. Interestingly, neither of these procedures caused any noticeable cytotoxicity. Next, cell loading with FITC-dextran and cell viability were systematically evaluated for different laser intensities (Figure 3). No appreciable cell loading occurred by AuNP or laser treatment alone. Instead, approximately 40% of the treated cells were loaded with FITC-dextran at a laser fluence of 0.38 J/cm^2. Increasing the laser fluence levels above the VNB threshold resulted in more positive cells and a much higher loading efficiency, as can be seen from the higher FITC-dextran signal per cell. At 2.04 J/cm^2 an optimum was found with >85% positive cells and a loading efficiency that is ~6 times higher than by AuNP heating at 0.38 J/cm^2. More levels of low laser fluence heating AuNP show no significant improvement of loading efficiency (Figure S4). There was no noticeable decrease in cell viability up to 2.04 J/cm^2. Further increasing the laser fluence to 4.08 J/cm^2 reduced the number of positive cells, likely due to the onset of cytotoxic effects as the VNBs are becoming rather large and damage the cells.[39] When increasing the AuNP concentration to 16.5 × 10^7 particles/mL, a similar trend was found, although here the percentage of positive and viable cells already decreased ~1.5 times at a laser fluence of 2.04 J/cm^2 (Figure S5). This shows that photoporation by VNBs also requires careful optimization of the concentration of AuNPs used. Based on these results, we decided to continue with 8.2 × 10^7 particles/mL, corresponding to approximately eight AuNPs per cell. These results obtained from confocal microscopy could be confirmed by flow cytometry analysis in a set of independent experiments (Figure S6). At 0.38 J/cm^2 ~50% of positive cells were found, while this increased to ~90% at 2.04 J/cm^2. The average intensity per cell

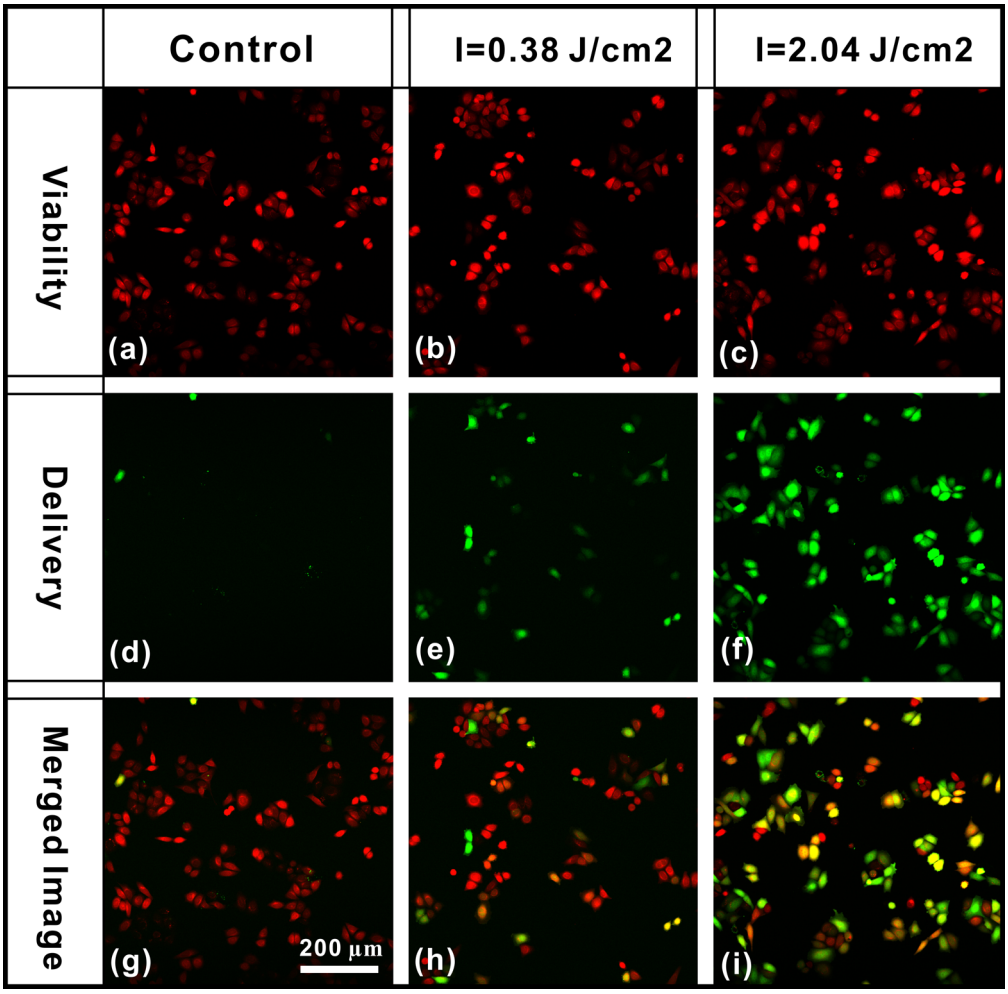

Figure 2. Confocal images showing the viability of HeLa cells labeled with calcein red-orange AM (a−c) and the intracellular delivery of FITC-dextran 10 kDa after laser treatment (d−f). The bottom row shows an overlay of both colors (g−i). At a laser fluence of 2.04 J/cm^2, VNBs are induced, which perforate the cell membrane and allow more efficient uptake of FITC-dextran as compared to a low laser fluence (0.38 J/cm^2), which causes heating of the AuNPs and the plasma membrane.

again increased by a factor of ~6, while no signs of cytotoxicity could be found.

To further evaluate the effect of the number of laser pulses on the delivery efficiency, the cells were scanned multiple times with pulsed laser illumination. As shown in Figure 4, no significant improvement of the loading efficiency was obtained for both direct heating and VNBs. This could be caused by melting of AuNPs and breaking up into smaller fragments.[47] Fragmentation of AuNPs has been reported at a laser fluence as low as 0.08 J/cm^2 for 40 nm particles.[48−50] On the basis of these results, we will perform further comparisons with single laser pulse treatment only.

Evaluation of Intracellular siRNA Delivery and Gene Silencing *via* Local Heating and VNB Generation. Next to the delivery of FITC-dextran as a model macromolecule, the applicability of photoporation for delivering macromolecular therapeutic agents, such as small interfering RNA, was assessed. Recently, siRNA was shown to be delivered into cells using AuNPs and photoporation by direct heating of the plasma membrane.[37] Considering our finding that VNBs are more efficient for loading cells with FITC-dextrans, we continued our comparative study toward siRNA gene silencing.

First, loading of HeLa cells with Alexa Fluor 488 (AF488)-labeled siRNA was evaluated by adding it to the cell medium prior to laser treatment. In analogy with previous experiments, the cells were incubated with a AuNP concentration of 8.25 × 10^7 particles/mL (*i.e.*, ~8 particles per cell). As shown in Figure S7, similar to our findings for FITC-dextran, direct heating of the plasma membrane (0.38 J/cm^2) is less efficient in delivering siRNA to the cytosol than pore formation by VNBs (2.04 J/cm^2). Cell viability and cellular delivery were again quantified by imaging processing (Figure S8). More than 90% of the cells were loaded with a detectable amount of siRNA with no signs of cytotoxicity at a laser fluence of 2.04 J/cm^2. Although heating of the plasma membrane also did not cause any cytotoxicity, the percentage of siRNA-containing cells was much less (~40%). Furthermore, the average fluorescence per cell

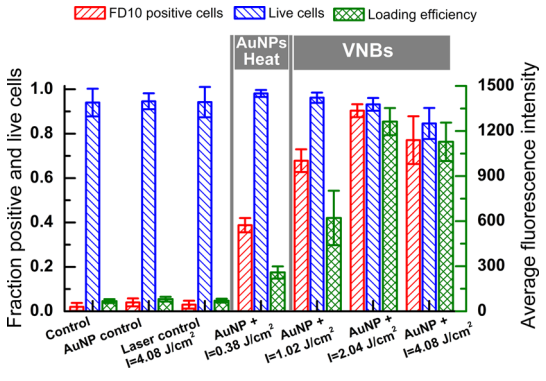

Figure 3. Cell viability and delivery efficiency of FITC-dextran 10 kDa (FD10) as quantified by imaging processing of confocal images. HeLa cells were incubated with 70 nm cationic AuNPs at a concentration of 8.25 × 10^7 particles/mL, corresponding to approximately eight AuNPs per cell. The laser fluence was adjusted to compare heating of the plasma membrane (0.38 J/cm^2) with pore formation by VNBs (1.02, 2.04, and 4.08 J/cm^2). Red bars are the fraction of FD10 positive cells, blue bars are the fraction of live cells, and olive bars are the average fluorescence intensity. The average FD10 fluorescence per cell is a measure of the loading efficiency. The data shown are the result from three independent experiments.

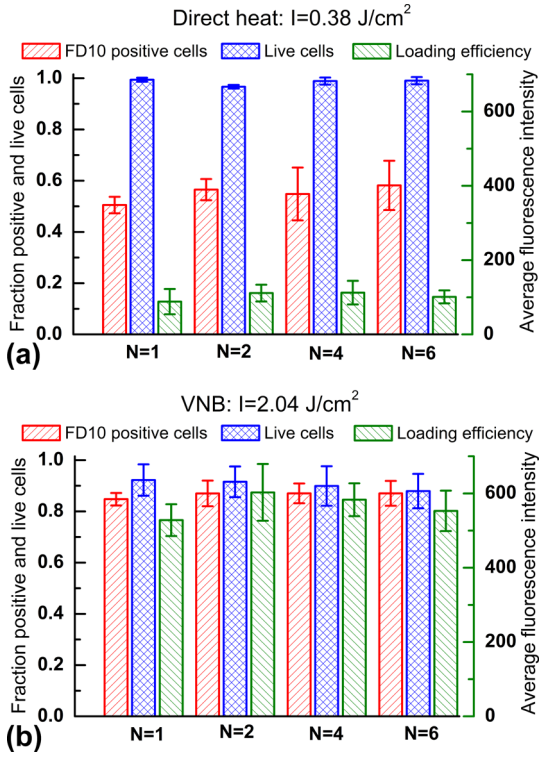

Figure 4. Positive cells, cell viability, and loading of FD10 using 8.25 × 10^7 AuNP/mL as a function of the number of laser pulses (N). Different laser fluences are compared: (a) 0.38 J/cm^2 (below the VNB threshold) and (b) 2.04 J/cm^2 (above the VNB threshold). No increase in loading efficiency is found by increasing the number of laser pulses for either condition.

was 4-fold higher in the case of VNB pore formation as compared to direct heating.

In a next step the knockdown efficiency of anti-EGFP siRNA delivered *via* the photoporation approach was evaluated in a human non-small-cell lung carcinoma cell line (H1299) that stably expresses EGFP. The knockdown efficiency and cell viability were measured by both confocal microscopy and flow cytometry. As shown in Figure 5a–c, the knockdown efficiency was about ~40% for direct heating of the plasma membrane (0.38 J/cm^2) as compared to >80% for VNB-induced pore formation (2.04 J/cm^2). No significant knockdown was observed in the case where the cells received exactly the same treatment (2.04 J/cm^2) but without AuNPs or when the same protocol was performed (~8 AuNPs per cell) but without laser exposure. Quantification of cell viability did not reveal any signs of cytotoxicity for any of the experiments. Taken together, it can be concluded that VNB-induced pore formation allows much more efficient cellular uptake of siRNA and target gene silencing as compared to cellular delivery *via* heating of the plasma membrane.

Tuning the Incident Laser Fluence Allows Size-Selective Intracellular Delivery. As demonstrated before, the size of a VNB is governed by the intensity of the incident laser beam.[32] Here we evaluated the hypothesis that the cell membrane pore size is thus also proportional to the incident laser fluence, meaning that large molecules can be delivered only *via* the pores formed by VNBs with a high intensity laser light, while smaller molecules can be delivered already at lower intensities such as for direct heating. To investigate this, immediately prior to the laser treatment, a mixture of two fluorescent dextrans of different molecular weight was added to HeLa cells, being red fluorescent 10 kDa Alexa-red dextran (RD10) and green fluorescent 500 kDa FITC-dextran (FD500). The cells were treated with a laser fluence of either 0.38 or 2.04 J/cm^2, after which the cells were washed and supplied with fresh cell medium. As can be seen from the confocal images in Figure 6a–c, at the lowest laser fluence the red fluorescent dextrans with low molecular weight could enter the cells quite efficiently. On the other hand, only a few cells had taken up the larger green fluorescent dextrans. At the highest laser fluence, clearly both small and large dextrans were delivered into the cells. By image analysis it was quantified that ~50% of treated cells were found to have taken up 10 kDa dextran at the lowest laser fluence, while this increased to ~90% at the highest laser fluence. However, for the larger 500 kDa dextrans less than 10% of the cells showed detectable uptake, which increased to >80% for the highest laser fluence. The average green fluorescence per cell for FD500 was only ~2-fold more than the control sample in the case of the lowest laser fluence, which increased to more than 10-fold at the highest laser fluence. Although more work is needed to investigate this relationship in more detail, these experiments show that the pore size can be easily changed by tuning the laser energy of the photoporation procedure.

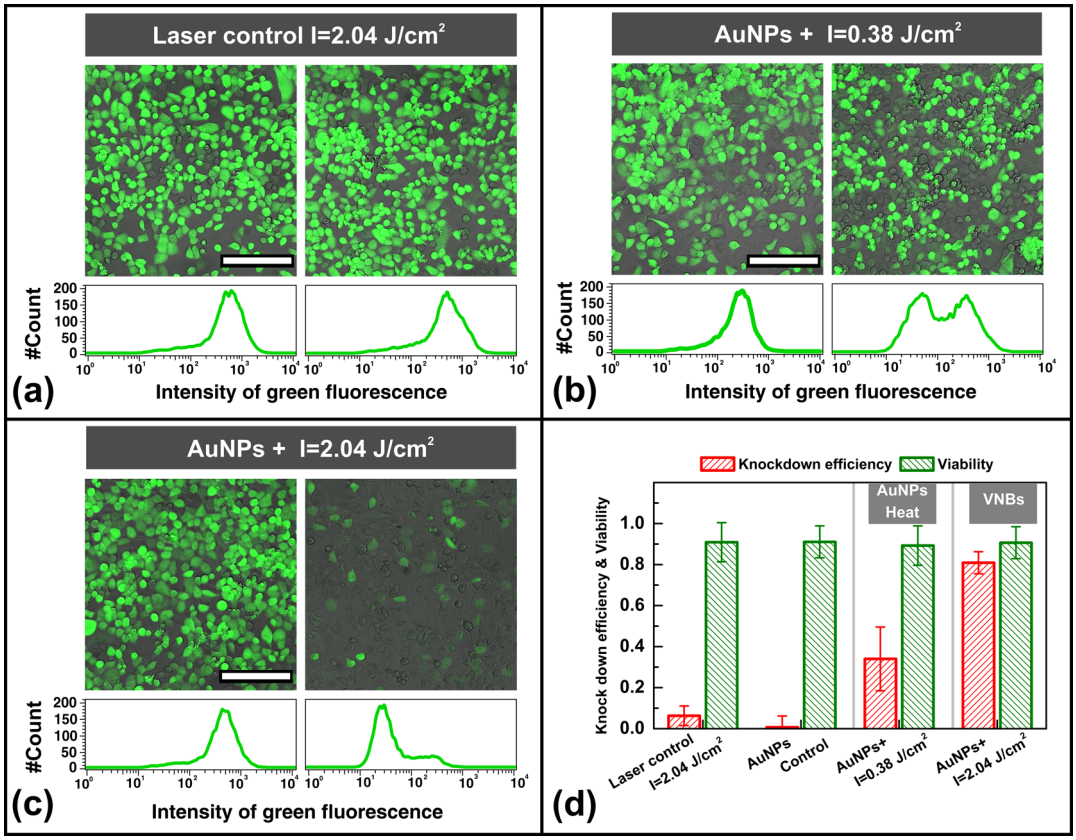

Figure 5. Photoporation of H1299 EGFP cells with varying laser intensity for siRNA gene silencing. Following the adsorption of AuNPs (positively charged, 70 nm, 8.25×10^7 particles/mL) to the cell surface, photoporation was initiated in the presence of siRNA. Twenty-four hours after treatment, the cellular EGFP expression was visualized by confocal microscopy and quantified with flow cytometry. The left and right microscopy images in (a)−(c) represent cells that are incubated with negative control siRNA and anti-EGFP siRNA, respectively, at a laser fluence of 2.04 J/cm² without incubation of AuNPs (a) and 0.38 J/cm² (b) and 2.04 J/cm² (c) with incubation of AuNPs. The corresponding flow cytometry histograms in (a)−(c) show the distributions of the cells' EGFP fluorescence. The cell viability and knockdown efficiency are quantified by flow cytometry (n = 3) (d). The scale bars shown in (a)−(c) correspond to 200 μm.

CONCLUSIONS

It was demonstrated that delivering macromolecules across the plasma membrane in cells is more efficient when pores are created by VNBs rather than by direct heating. This is likely caused by a larger pore size in the case of VNBs, due to which more molecules can diffuse into the cell. When delivering siRNA, this might result in more efficient gene knockdown as well. Despite the fact that VNB generation requires a higher laser energy, it did not result in increased toxicity. This is likely due to the fact that VNB generation is an almost purely mechanical effect that does not lead to heat diffusion into the surrounding tissue. Interestingly, by tuning the laser energy and hence the size of the VNBs, it is possible to tune the size of the pores that are created. This in turn allows controlling the amount of molecules that are delivered into the cytosol, as well as the maximum size of molecules that are allowed to pass through. Combined with the general applicability of the approach and the fact that this procedure can be applied to large cell numbers by scanning of the laser beam, we are convinced that VNB photoporation is a promising alternative physical technique to efficiently deliver compounds into cells with little or no toxicity. In future research it will be of interest to further investigate the influence of AuNP size and cell type on pore size and drug delivery efficiency.

MATERIALS AND METHODS

Materials. Cationic AuNPs of 70 nm were purchased from NanoPartz (#C2159, Nanopartz Inc., Loveland, CO, USA). These AuNPs had a zeta potential of 30 mV as measured by dynamic light scattering (NanoSizer, Malvern, UK). FITC-dextrans with M_w's of 10 and 500 kDa were purchased from Sigma-Aldrich (Belgium). Calcein red-orange AM (#C34851, CellTrace) and Alexa Fluor 647 labeled dextran of 10 kDa (#D-22914) were obtained from Invitrogen (Belgium). Twenty-one-nucleotide siRNA duplexes targeting the enhanced green fluorescent protein (siEGFP) and negative control duplexes (siCTRL) were purchased from Eurogentec (Seraing, Belgium). siEGFP: sense strand = 5′-CAAGCUGACCCUGAAGUUC**tt**-3′; antisense strand = 5′-GAACUUCAGGGUCAGCUUG**tt**-3′. siCTRL: sense

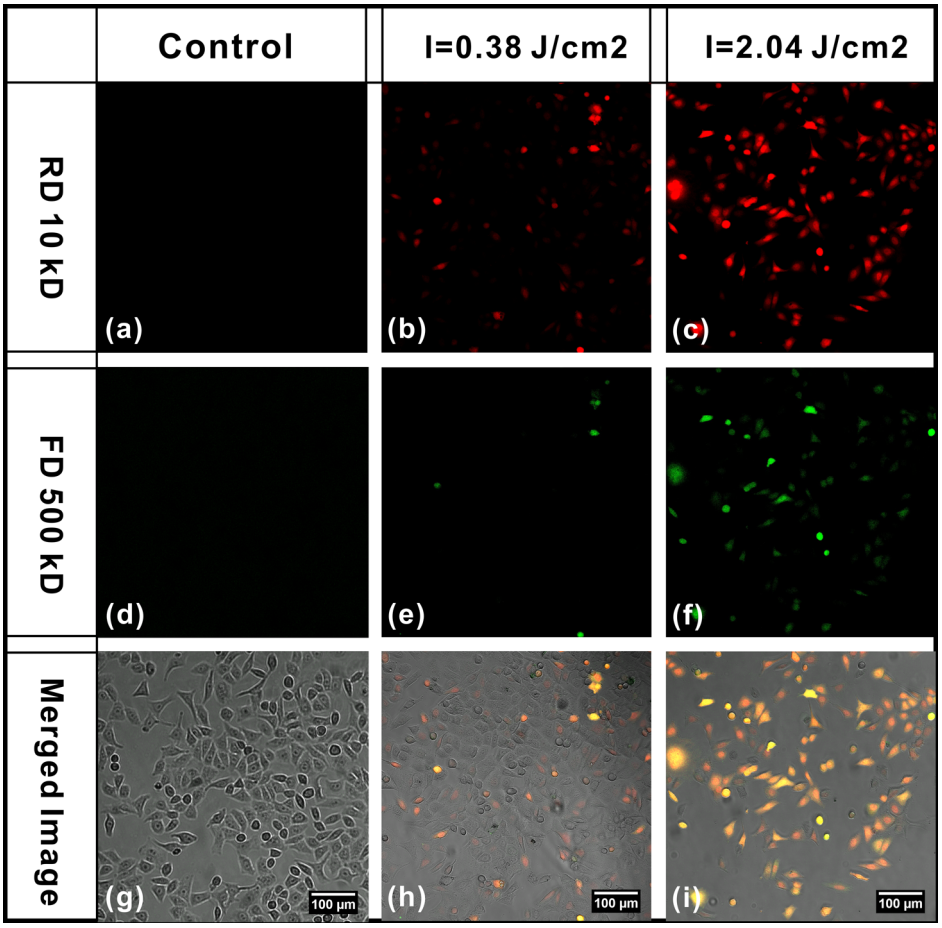

Figure 6. Size-selective delivery of fluorescently labeled dextrans is demonstrated in HeLa cells. Cells are supplied with a mixture of red fluorescent Alexa-red dextran of 10 kDa (RD10) and green fluorescent FITC-dextran of 500 kDa (FD500). (a–c) Confocal images showing the delivery of RD10 in HeLa cells that received laser treatment of 0.38 or 2.04 J/cm^2. (d–f) Confocal images showing the delivery of FD500. (g–i) Merged confocal images of green and red fluorescence with transmission images.

strand = 5′-UGCGCUACGAUCGACGAUG**tt**-3′; antisense strand = 5′-CAUCGUCGAUCGUAGCGCA**tt**-3′ (lower case bold letters represent 2′-deoxyribonucleotides, capital letters are ribonucleotides). For fluorescence experiments, the siCTRL duplex was labeled with a Cy5 dye at the 5′ end of the sense strand (Eurogentec).

Cell Experiments. HeLa cells as a generally used cell model were employed in this study, and H1299 cells stably expressing EGFP were used for siRNA knockdown experiment. Before laser treatment, HeLa cells (1×10^4 cells/well) were grown in cell medium of DMEM/F-12 with 2 mM glutamine, 10% heat-inactivated fetal bovine serum (FBS, Hyclone), and 100 U/mL penicillin/streptomycin, and H1299_EGFP cells (1×10^4 cells/well) were cultured in 96 wells (#92096, TPP, Switzerland) at 37 °C in RPMI 1640, supplemented with 2 mM glutamine, 10% heat-inactivated FBS, and 100 U/mL penicillin/streptomycin at 37 °C in a humidified atmosphere containing 5% CO_2 for 24 h before treatment. For laser treatment, the cells were incubated with AuNPs for 30 min at concentrations as indicated in the text. Following incubation with AuNPs, the cells were washed to remove any remaining free AuNPs in solution. Just prior to the laser scanning treatment, the solution of extracellular agents (dextrans or siRNA) was added to the cells. After the laser treatment, the cells were washed and supplied with fresh cell medium. CellTrace calcein red-orange AM was added to the samples for 45 min incubation at room temperature to stain living cells to quantify cell viability. Images of the prepared cell samples were taken by confocal microscope (C1-si, Nikon, Japan) to quantify the molecular loading efficiency and cell viability. The samples were also prepared for measurement by flow cytometer. The cells were washed with PBS, trypsinized (trypsin/EDTA 0.25%), and diluted with complete cell culture medium. Following centrifugation (7 min, 300*g*), the cell pellet was resuspended in flow buffer (PBS supplemented with 1% BSA and 0.1% sodium azide), and placed on ice until flow cytometric analysis. A minimum of 10^4 cells were analyzed in each measurement, using a BD Biosciences FACSCalibur flow cytometer.

Generation and Detection of AuNP Heating and VNB Formation. A homemade setup including an optical system and electric timing system was used to generate and detect the AuNP heating or VNBs. As shown in Figure S2, a pulsed laser with a pulse duration of ~7 ns was tuned at a wavelength of 561 nm (Opolette HE 355 LD, OPOTEK Inc., CA, USA) and used for illumination of AuNPs. The setup has two modes for detecting AuNP heating or VNB formation, respectively. The time-response mode is used for detecting both of AuNP heating and VNBs. It makes use of a photodetector (APD110A, Thorlabs) that monitors a change in transmitted light of a CW red laser (Spectra-Physics Excelsion-640, Santa Calara, CA, USA) due to changes in refractive index upon heating.[43] VNBs on the other hand can be very well detected by dark-field microscopy, as they efficiently scatter light. As VNBs typically have a very short lifetime (<1 μs), depending on their size, we synchronized the camera (EMCCD camera, Cascade II: 512, Photometrics, Tucson, AZ, USA) with the pulsed laser by an electronic pulse generator (BNC575, Berkeley Nucleonics Corporation, CA, USA). The pulse laser sends a Q-switch signal to trigger the pulse generator, and it will trigger the camera at a setting delay.

For treating large areas of cells, such as an entire well of a 96-well plate, an electronic microscope stage was used to scan

the laser beam (20 Hz pulse frequency) line by line across the entire sample. The scanning speed was 2 mm/s, and the distance between subsequent lines was 0.1 mm (diameter of the laser beam). This way each location in the sample receives a single laser pulse, with a total treatment time of ~3.6 min per well. The laser pulse energy was monitored by an energy meter (J-25MB-HE&LE, Energy Max-USB/RS sensors, Coherent) synchronized with the pulsed laser. The intensity of the exciting pulse laser was calculated as the average pulse energy divided by the area of the laser beam. Individual pulses were observed to deviate up to 10% from the average value.

Quantification of Cell Loading and Viability. After laser treatment, at least five confocal images were acquired with a confocal laser scanning microscope (C1si, Nikon, Japan). Using a 10× lens (CFI Plan Apochromat, Nikon, Badhoevedorp, The Netherlands), each image had a field of view of 1.35 mm by 1.35 mm with several hundreds to a thousand cells for each image. Each image consisted of three channels, one for green fluorescence (505−550 nm), one for orange-red fluorescence (575−620 nm), and one for the transmission image. A Matlab (The Matworks, Natick, MA, USA) program was written for automated quantification of cell loading and cell viability. First, the average intensity per cell was measured in both fluorescence channels. Green fluorescence resembles cell loading, and orange-red fluorescence is used for quantifying cell viability. Untreated cells are used to define the threshold for positive cell loading, where the threshold value is defined as the 95% level of untreated cells. Similarly, cells are considered alive when the orange-red fluorescence intensity is higher than the 95% level of dead cells.

For calculating siRNA gene silencing efficiency, EGFP knockdown efficiency was quantified as the average fluorescence intensity of cells treated with anti-EGFP siRNA divided by the average intensity of cells treated with negative control siRNA under identical experimental conditions as the following equation:

$$\text{Knockdown effficiency } (\%) = 1 - \frac{\text{MFI siEGFP}}{\text{MFI siCTRL}} \times 100\%$$

with MFI siEGFP indicating the mean fluorescence intensity of cells incubated with anti-EGFP siRNA and MFI siCTRL indicating the mean fluorescence intensity of cells incubated with negative control siRNA.

For flow cytometry, data analysis was performed by using the BD CellQuest Pro analysis software.

Conflict of Interest: The authors declare no competing financial interest.

Acknowledgment. Financial support by the Ghent University Special Research Fund (Centre for Nano- and Biophotonics) is acknowledged with gratitude. R.X. gratefully acknowledges the financial support from China Scholarship Council (CSC). K.R. and I.L. are postdoctoral fellows of the Research Foundation-Flanders (FWO-Vlaanderen).

Supporting Information Available: Additional figures as described in the text. This material is available free of charge *via* the Internet at http://pubs.acs.org.

REFERENCES AND NOTES

1. Mann, S. Life as a Nanoscale Phenomenon. *Angew. Chem., Int. Ed.* **2008**, *47*, 5306–5320.
2. Davidson, B. L.; McCray, P. B., Jr. Current Prospects for RNA Interference-Based Therapies. *Nat. Rev. Gene* **2011**, *12*, 329–340.
3. Varkouhi, A. K.; Scholte, M.; Storm, G.; Haisma, H. J. Endosomal Escape Pathways for Delivery of Biologicals. *J. Controlled Release* **2011**, *151*, 220–228.
4. Raemdonck, K.; Naeye, B.; Hogset, A.; Demeester, J.; De Smedt, S. C. Prolonged Gene Silencing by Combining Sirna Nanogels and Photochemical Internalization. *J. Controlled Release* **2010**, *145*, 281–288.
5. Prentice, P.; Cuschierp, A.; Dholakia, K.; Prausnitz, M.; Campbell, P. Membrane Disruption by Optically Controlled Microbubble Cavitation. *Nat. Phys.* **2005**, *1*, 107–110.
6. Mehier-Humbert, S.; Guy, R. H. Physical Methods for Gene Transfer: Improving the Kinetics of Gene Delivery into Cells. *Adv. Drug Deliver Rev.* **2005**, *57*, 733–753.
7. Lai, B. H.; Chen, D. H. Lab6 Nanoparticles with Carbon-Doped Silica Coating for Fluorescence Imaging and Near-IR Photothermal Therapy of Cancer Cells. *Acta Biomater.* **2013**, *9*, 7556–7563.
8. Auerbach, A. B. Production of Functional Transgenic Mice by DNA Pronuclear Microinjection. *Acta Biochim. Polym.* **2004**, *51*, 9–31.
9. Gordon, J. W.; Scangos, G. A.; Plotkin, D. J.; Barbosa, J. A.; Ruddle, F. H. Genetic-Transformation of Mouse Embryos by Micro-Injection of Purified DNA. *Proc. Natl. Acad. Sci.-Biol.* **1980**, *77*, 7380–7384.
10. Capecchi, M. R. High-Efficiency Transformation by Direct Micro-Injection of DNA into Cultured Mammalian-Cells. *Cell* **1980**, *22*, 479–488.
11. Murphy, R. C.; Messer, A. Gene Transfer Methods for CNS Organotypic Cultures: A Comparison Three Nonviral Methods. *Mol. Ther.* **2001**, *3*, 113–121.
12. Canatella, P. J.; Prausnitz, M. R. Prediction and Optimization of Gene Transfection and Drug Delivery by Electroporation. *Gene Ther.* **2001**, *8*, 1464–1469.
13. Goto, T.; Nishi, T.; Tamura, T.; Dev, S. B.; Takeshima, H.; Kochi, M.; Yoshizato, K.; Kuratsu, J.; Sakata, T.; Hofmann, G. A.; *et al*. Highly Efficient Electro-Gene Therapy of Solid Tumor by Using an Expression Plasmid for the Herpes Simplex Virus Thymidine Kinase Gene. *Proc. Natl. Acad. Sci. U.S.A.* **2000**, *97*, 354–359.
14. Mir, L. M.; Bureau, M. F.; Gehl, J.; Rangara, R.; Rouy, D.; Caillaud, J. M.; Delaere, P.; Branellec, D.; Schwartz, B.; Scherman, D. High-Efficiency Gene Transfer into Skeletal Muscle Mediated by Electric Pulses. *Proc. Natl. Acad. Sci. U.S.A.* **1999**, *96*, 4262–4267.
15. Muramatsu, T.; Mizutani, Y.; Ohmori, Y.; Okumura, J. Comparison of Three Nonviral Transfection Methods for Foreign Gene Expression in Early Chicken Embryos in Ovo. *Biochem. Biophys. Res. Commun.* **1997**, *230*, 376–380.
16. Yi, J.; Barrow, A. J.; Yu, N.; O'Neill, B. E. Efficient Electroporation of Liposomes Doped with Pore Stabilizing Nisin. *J. Liposome Res.* **2013**, *23*, 197–202.
17. Rubinsky, B. Irreversible Electroporation in Medicine. *Technol. Cancer Res. Treat.* **2007**, *6*, 255–260.
18. Lentacker, I.; De Cock, I.; Deckers, R.; De Smedt, S. C.; Moonen, C. T. W. Understanding Ultrasound Induced Sonoporation: Definitions and Underlying Mechanisms. *Adv. Drug Delivery Rev.* **2014**, *72*, 49–64.
19. Lentacker, I.; De Smedt, S. C.; Sanders, N. N. Drug Loaded Microbubble Design for Ultrasound Triggered Delivery. *Soft Matter* **2009**, *5*, 2161–2170.
20. Lakshmanan, S.; Gupta, G. K.; Avci, P.; Chandran, R.; Sadasivam, M.; Jorge, A. E.; Hamblin, M. R. Physical Energy for Drug Delivery; Poration, Concentration and Activation. *Adv. Drug Delivery Rev.* **2014**, *71*, 98–114.
21. Park, D.; Ryu, H.; Kim, H. S.; Kim, Y. S.; Choi, K. S.; Park, H.; Seo, J. Sonophoresis Using Ultrasound Contrast Agents for Transdermal Drug Delivery: An *in Vivo* Experimental Study. *Ultrasound Med. Biol.* **2012**, *38*, 642–650.
22. Wu, T. H.; Chen, Y.; Park, S. Y.; Hong, J.; Teslaa, T.; Zhong, J. F.; Di Carlo, D.; Teitell, M. A.; Chiou, P. Y. Pulsed Laser Triggered High Speed Microfluidic Fluorescence Activated Cell Sorter. *Lab Chip* **2012**, *12*, 1378–1383.
23. Sibbett, W.; Lagatsky, A. A.; Brown, C. T. A. The Development and Application of Femtosecond Laser Systems. *Opt Express* **2012**, *20*, 6989–7001.
24. Baumgart, J.; Humbert, L.; Boulais, E.; Lachaine, R.; Lebrun, J. J.; Meunier, M. Off-Resonance Plasmonic Enhanced Femtosecond Laser Optoporation and Transfection of Cancer Cells. *Biomaterials* **2012**, *33*, 2345–2350.
25. Stevenson, D. J.; Gunn-Moore, F. J.; Campbell, P.; Dholakia, K. Single Cell Optical Transfection. *J. R Soc. Interface* **2010**, *7*, 863–871.
26. Chakravarty, P.; Qian, W.; El-Sayed, M. A.; Prausnitz, M. R. Delivery of Molecules into Cells Using Carbon Nanoparticles

Activated by Femtosecond Laser Pulses. *Nat. Nanotechnol.* **2010**, *5*, 607–611.
27. Jain, T.; Muthuswamy, J. Bio-Chip for Spatially Controlled Transfection of Nucleic Acid Payloads into Cells in a Culture. *Lab Chip* **2007**, *7*, 1004–1011.
28. Tirlapur, U. K.; Konig, K. Cell Biology - Targeted Transfection by Femtosecond Laser. *Nature* **2002**, *418*, 290–291.
29. Sapsford, K. E.; Algar, W. R.; Berti, L.; Gemmill, K. B.; Casey, B. J.; Oh, E.; Stewart, M. H.; Medintz, I. L. Functionalizing Nanoparticles with Biological Molecules: Developing Chemistries that Facilitate Nanotechnology. *Chem. Rev.* **2013**, *113*, 1904–2074.
30. Qin, Z. P.; Bischof, J. C. Thermophysical and Biological Responses of Gold Nanoparticle Laser Heating. *Chem. Soc. Rev.* **2012**, *41*, 1191–1217.
31. Zijlstra, P.; Orrit, M. Single Metal Nanoparticles: Optical Detection, Spectroscopy and Applications. *Rep. Prog. Phys.* **2011**, 74.
32. Lapotko, D. Optical Excitation and Detection of Vapor Bubbles around Plasmonic Nanoparticles. *Opt. Express* **2009**, *17*, 2538–2556.
33. Ghosh, S. K.; Pal, T. Interparticle Coupling Effect on the Surface Plasmon Resonance of Gold Nanoparticles: From Theory To Applications. *Chem. Rev.* **2007**, *107*, 4797–4862.
34. Skirtach, A. G.; Dejugnat, C.; Braun, D.; Susha, A. S.; Rogach, A. L.; Parak, W. J.; Mohwald, H.; Sukhorukov, G. B. The Role of Metal Nanoparticles in Remote Release of Encapsulated Materials. *Nano Lett.* **2005**, *5*, 1371–1377.
35. Sun, X. H.; Zhang, G. D.; Keynton, R. S.; O'Toole, M. G.; Patel, D.; Gobin, A. M. Enhanced Drug Delivery *via* Hyperthermal Membrane Disruption Using Targeted Gold Nanoparticles with Pegylated Protein-G as a Cofactor. *Nanomed. Nanotechnol. Biol. Med.* **2013**, *9*, 1214–1222.
36. Kalies, S.; Heinemann, D.; Schomaker, M.; Birr, T.; Ripken, T.; Meyer, H. Gold Nanoparticle Mediated Laser Transfection for High-Throughput Antisense Applications. *Proc. SPIE* **2013**, 8803.
37. Heinemann, D.; Schomaker, M.; Kalies, S.; Schieck, M.; Carlson, R.; Escobar, H. M.; Ripken, T.; Meyer, H.; Heisterkamp, A. Gold Nanoparticle Mediated Laser Transfection for Efficient siRNA Mediated Gene Knock Down. *PLoS One* **2013**, 8.
38. Delcea, M.; Sternberg, N.; Yashchenok, A. M.; Georgieva, R.; Baumler, H.; Mohwald, H.; Skirtach, A. G. Nanoplasmonics for Dual-Molecule Release through Nanopores in the Membrane of Red Blood Cells. *ACS Nano* **2012**, *6*, 4169–4180.
39. Lukianova-Hleb, E. Y.; Mutonga, M. B. G.; Lapotko, D. O. Cell-Specific Multifunctional Processing of Heterogeneous Cell Systems in a Single Laser Pulse Treatment. *ACS Nano* **2012**, *6*, 10973–10981.
40. Lapotko, D. Plasmonic Nanoparticle-Generated Photothermal Bubbles and Their Biomedical Applications. *Nanomedicine (London, U.K.)* **2009**, *4*, 813–845.
41. Lukianova-Hleb, E. Y.; Wagner, D. S.; Brenner, M. K.; Lapotko, D. O. Cell-Specific Transmembrane Injection of Molecular Cargo with Gold Nanoparticle-Generated Transient Plasmonic Nanobubbles. *Biomaterials* **2012**, *33*, 5441–5450.
42. Lukianova-Hleb, E. Y.; Ren, X. Y.; Zasadzinski, J. A.; Wu, X. W.; Lapotko, D. O. Plasmonic Nanobubbles Enhance Efficacy and Selectivity of Chemotherapy against Drug-Resistant Cancer Cells. *Adv. Mater.* **2012**, *24*, 3831–3837.
43. Zharov, V. P.; Lapotko, D. O. Photothermal Imaging of Nanoparticles and Cells. *IEEE J. Sel. Top. Quantum Electron.* **2005**, *11*, 733–751.
44. Lukianova-Hleb, E. Y.; Lapotko, D. O. Influence of Transient Environmental Photothermal Effects on Optical Scattering by Gold Nanoparticles. *Nano Lett.* **2009**, *9*, 2160–2166.
45. Huhn, D.; Govorov, A.; Gil, P. R.; Parak, W. J. Photostimulated Au Nanoheaters in Polymer and Biological Media: Characterization of Mechanical Destruction and Boiling. *Adv. Funct. Mater.* **2012**, *22*, 294–303.
46. Yamane, D.; Wu, Y. C.; Wu, T. H.; Toshiyoshi, H.; Teitell, M. A.; Chiou, P. Y. Electrical Impedance Monitoring of Photothermal Porated Mammalian Cells. *J. Lab. Autom.* **2014**, *19*, 50–59.
47. Yao, C. P.; Qu, X. C.; Zhang, Z. X.; Huttmann, G.; Rahmanzadeh, R. Influence of Laser Parameters on Nanoparticle-Induced Membrane Permeabilization. *J. Biomed. Opt.* **2009**, 14.
48. Kotaidis, V.; Plech, A. Cavitation Dynamics on the Nanoscale. *Appl. Phys. Lett.* **2005**, 87.
49. Takami, A.; Kurita, H.; Koda, S. Laser-Induced Size Reduction of Noble Metal Particles. *J. Phys. Chem. B* **1999**, *103*, 1226–1232.
50. Kurita, H.; Takami, A.; Koda, S. Size Reduction of Gold Particles in Aqueous Solution by Pulsed Laser Irradiation. *Appl. Phys. Lett.* **1998**, *72*, 789–791.